Hyperspectral Unmixing for Remote Sensing of Unresolved Objects

Miguel Velez-Reyes, Jiarui Yi
Sensor and Signal Analytics Laboratory
Department of Electrical and Computer Engineering,
The University of Texas at El Paso, 500 W University Ave, El Paso, TX, USA 79968
E-mail: mvelezreyes@utep.edu, jyi2@utep.edu

ABSTRACT

This paper studies at the application of unmixing to hyperspectral remote sensing of unresolved objects for space situational awareness. We review library-based unmixing and its application for hyperspectral remote sensing of unresolved objects. The concept of spectro-temporal signatures is introduced and its potential value for unsupervised unmixing of unresolved objects is discussed. Data-driven endmember extraction algorithms from terrestrial applications are applied to data sets generated using simulations. We study the limitations of unsupervised hyperspectral methods for extracting material composition of unresolved space object. Results show that data driven approached may not work with the small size of temporal spectral traces of unresolved space objects and they may not be informative enough for endmember extraction.

Keywords: Hyperspectral remote sensing, Unresolved resident space objects, Spectro-temporal signatures, Space situational awareness. Endmember extraction.

1. INTRODUCTION

The United States depends economically and militarily in its space assets [1]. Satellites provide a multitude of critical services, which are critical for US defense, security and economic wealth. Space situational awareness (SSA) is needed to have a clear picture of the environment surrounding US space assets to detect any changes or potential threats. The increase of space assets and of debris caused by man-made objects that no longer serve a useful purpose, require remote sensing technologies to support collision avoidance and catalog maintenance as well as to support a more tactical, predictive, and intelligence driven SSA.

Radar ground assets are primarily used for observing targets in Low Earth Orbit while optical ground assets are used to assess the environment at higher altitudes. Current ground-based space telescope technology cannot spatially resolve objects in space that are distant (e.g. GEO) or that are small (e.g. CubeSats, orbital debris). These are denoted as unresolved resident space objects (URSO). Current technology only allows to qualitatively assess the risk from objects in Earth orbit [2].

One approach that can potentially extract quantitative information about URSO is hyperspectral remote sensing. The high spectral resolution of hyperspectral imagers allows extraction information about the material composition of unresolved objects from their contribution to the measured mixed spectra [3]. Thus, hyperspectral remote sensing can provide a quantitative approach to assessing/extracting URSO material composition information. Even though the object cannot be spatially resolved, it may be spectrally resolved.

The paper is organized as follows. Section 2 presents a brief introduction to linear spectral mixing and unmixing. Section 3 presents experiments on endmember extraction from simulated mixed spectral temporal traces. We see that data-driven approached may not have the capability to extract material composition information if the spectral trace data is not informative enough. Section present discussion and final remarks.

2. HYPERSPECTRAL UNMIXING

A standard model for spectral mixing is the linear mixing model (LMM) where the measured mixed spectral signature, $\boldsymbol{x} \in \mathfrak{R}_+^m$ is represented as a convex linear combination of the endmember spectral signatures $\boldsymbol{s}_i \in \mathfrak{R}_+^m$ [4].

$$\boldsymbol{x} = \sum_{i=1}^{p} a_i \boldsymbol{s}_i + \boldsymbol{w} = \boldsymbol{S}\boldsymbol{a} + \boldsymbol{w} \quad (1)$$

where p is the number of endmembers, m is the number of bands, $\boldsymbol{w} \in \Re^{\boldsymbol{m}}$ is the vector of noise, a_i is the i-th endmember fractional abundance, $\boldsymbol{S} = [\boldsymbol{s}_1 \quad \boldsymbol{s}_2 \quad \cdots \quad \boldsymbol{s}_p] \in \Re_+^{m \times p}$ is the matrix of endmembers, and $\boldsymbol{a} \in \Re_+^{p}$ is the vector of abundances. Here $\Re_+^m$ denotes the positive orthant of $\Re^{\boldsymbol{m}}$. Since abundances a_i are related to the fraction of area covered by the material in the field of view of the sensor they need to satisfy $a_i \geq 0$, and $\boldsymbol{a}^T \boldsymbol{1} = \sum_{i=1}^{p} a_i = 1$. This later constraint is called the sum-to-one constraint (STO) imposed on the abundances.

A SSA hyperspectral remote sensor such as Spica [5] or SpeX [6] collect spectral reflectance traces of a space object over a specific period of time. As the object rotates or tumbles different faces of the URSO are in the field of view of the sensor. The signature on each pixel of the trace is a mixture of the signatures of the URSO materials in the field of view of the sensor at that instant of time. Let $\boldsymbol{X} = [\boldsymbol{x}_1 \quad \boldsymbol{x}_2 \quad \cdots \quad \boldsymbol{x}_N] \in \Re_+^{m \times N}$ be the matrix of measured spectral signatures in a time trace. We will call this matrix the spectro-temporal signature of the URSO that can be used to restate (1) in matrix form as follow

$$\boldsymbol{X} = \boldsymbol{S}\boldsymbol{A} + \boldsymbol{W} \quad (2)$$

where $\boldsymbol{S} = [\boldsymbol{s}_1 \quad \boldsymbol{s}_2 \quad \cdots \quad \boldsymbol{s}_p] \in \Re_+^{m \times p}$ is the matrix of spectral signatures of the material in the URSO (or endmembers), $\boldsymbol{A} = [\boldsymbol{a}_1 \quad \boldsymbol{a}_2 \quad \cdots \quad \boldsymbol{a}_N] \in \Re_+^{p \times N}$ is the matrix of endmember abundances, $\boldsymbol{W} = [\boldsymbol{w}_1 \quad \boldsymbol{w}_2 \quad \cdots \quad \boldsymbol{w}_N] \in \Re_+^{m \times N}$ is the noise matrix, and N is the number of measured spectral signatures in the temporal trace. The spectro-temporal signature could be exploited by unmixing procedures to extract URSO material composition information that can be used for object tracking and identification.

The *hyperspectral unmixing problem* refers to the problem of finding the number of endmembers p, their spectral signatures $\boldsymbol{s}_i$, and their abundances a_i for $i = 1,2, \ldots, p$. This is an ill-posed problem. Estimating the number of endmembers p and finding their spectral signatures are the main challenges in unmixing. Furthermore note that (3) does not account for variability of spectral endmembers as an endmember is represented by a single spectral signature.

Additional constraints are included in unmixing process to obtain physically meaningful solutions. For instance, equations (1) and (2) combined with the abundance constraints suggests that the measured mixed spectra **x** is inside a simplex with corners at the endmember signatures [4]. This geometric constraint is an important constraint that motivates many of the endmember extraction approaches used in hyperspectral unmixing that aim at finding the corners of the smallest simplex enclosing the hyperspectral data cloud.

2.1 Abundance Estimation

If the number endmembers p and their spectral signatures $\boldsymbol{s}_i$ are known, the unmixing problem reduces to the *abundance estimation* problem (AEP) given by

$$\hat{\boldsymbol{a}}_{FC} = \arg\min \|\boldsymbol{x} - \boldsymbol{S}\boldsymbol{a}\|_2^2 \qquad \text{subject to } \boldsymbol{a} \in \Re_+^p, \ \boldsymbol{a}^T \boldsymbol{1} = 1 \quad (3)$$

A common assumption is that $p < m$. Notice that (3) is a constrained linear least squares (CLLS) problem. The constraints are inequality constraints because of the non-negativity of abundances and equality constraints due to the sum-to-one requirement for fractional abundances. In the unmixing literature, (3) is referred to as the fully constrained LLS (FCLLS) abundance estimation problem. Algorithms to solve the FCLLS and their application to abundance estimation in hyperspectral unmixing are discussed in [4].

Simpler abundance estimation algorithms result by enforcing some or none of the constraints. For instance, an unconstrained least squares (ULS) problem results when none of the constraints in (3) are enforced. The ULS has a close-form solution given by

$$\hat{\boldsymbol{a}}_{ULS} = (\boldsymbol{S}^T \boldsymbol{S})^{-1} \boldsymbol{S}^T \boldsymbol{x} \quad (4)$$

The unconstrained solution can be quite useful in assessing the quality of the linear mixing model. In the noise free case and under perfect modeling in (1), we have that $\hat{\boldsymbol{a}}_{UC} = \hat{\boldsymbol{a}}_{FC}$. Constraint enforcement is necessary due to noise. The closeness of $\hat{\boldsymbol{a}}_{UC}$ to $\hat{\boldsymbol{a}}_{FC}$ could be used as a diagnostic for the quality of the extracted linear mixing model for a particular mixed signature.

If only the sum-to-one constraint is enforced, a close form solution is also possible and is given by

$$\hat{\boldsymbol{a}}_{STO} = \hat{\boldsymbol{a}}_{ULS} + (\boldsymbol{S}^T\boldsymbol{S})^{-1}\varphi\mathbf{1} \tag{5}$$

where

$$\varphi = \frac{1 - \mathbf{1}^T\hat{\boldsymbol{a}}_{ULS}}{\mathbf{1}^T(\boldsymbol{S}^T\boldsymbol{S})^{-1}\mathbf{1}}$$

and $\mathbf{1}$ is a vector of ones. If only the non-negative constraint is enforced, the resulting problem is called the non-negative least squares (NNLS) problem for which the iterative algorithm presented in [7] is widely used and available in the MATLAB and in the GNU-Octave software. Multiplicative iterative algorithms can be used to solve the NNLS problem as described in [8].

The AEP produces accurate results in the noise free case if the correct endmembers are in $\boldsymbol{S}$. Note that if the number of endmembers or their signatures are incorrect, the optimization routine used to solve (1) will produce a numerical solution that gives an incorrect characterization of the mixed spectral signature $\boldsymbol{x}$.

2.2 Library-Based Unmixing

Library-based unmixing is a common technique for hyperspectral unmixing. Spectral libraries can be developed from field, image-derived and/or laboratory spectra. Examples of spectral libraries used for hyperspectral unmixing are the USGS spectral library [9], the JPL ASTER Spectral Library [10], and the NASA Spectral Database at NASA\JSC [11]. This later one has been used in SSA unmixing applications.

The *Multiple Endmember Spectral Mixture Analysis* (MESMA) [12] seeks to finds the likely composition of each mixed pixel by selecting subsets of endmembers from the spectral library and fitting them to the measured spectra $\boldsymbol{x}$ by solving (3) for each combination. The endmember subset that produces the lowest fitting error is chosen as the most likely one. MESMA assumes that the number of endmember in a mixed pixel is small (2 to 4) and tests for a large number of possible models with 2-4 endmembers until a suitable one is found.

Another approach to library-based unmixing is based on sparse regression (SR). This approach jointly estimates the number of endmembers and extracts their abundances from the data without performing a combinatorial search. In sparse regression unmixing, the following optimization problem is solved [13]

$$\hat{\bar{\boldsymbol{a}}} = \arg\min \|\bar{\boldsymbol{a}}\|_0 \qquad \text{subject to } \|\boldsymbol{x} - \bar{\boldsymbol{S}}\bar{\boldsymbol{a}}\|_2 \leq \delta \tag{6}$$

where $\| \ \|_0$ is the nuclear norm and it denotes the number of nonzero elements in $\bar{\boldsymbol{a}} \in \mathfrak{R}_+^L$, $\bar{\boldsymbol{S}} = [\boldsymbol{s}_1 \quad \boldsymbol{s}_2 \quad \cdots \quad \boldsymbol{s}_L] \in \mathfrak{R}_+^{m\times L}$ is the matrix of all spectral signatures in the spectral library, and L is the number of spectral signatures in the library. In most applications, $L >> p$. Note that once (6) is solved $\|\hat{\bar{\boldsymbol{a}}}\|_0 = \hat{p}$ and the non-zero elements of $\hat{\bar{\boldsymbol{a}}}$ identify the selected spectral signatures and their values are estimates of their abundances. The $\| \ \|_0$ is discrete and non-convex which results in (6) being NP-hard. In most SR applications, a relaxed version of (6) is solved where $\| \ \|_0$ is replaced by $\| \ \|_1$ making (6) a convex optimization problem. The convex approximation produces a satisfactory sparse solution under mild conditions [13].

Library-based unmixing has been used in SSA. For instance, [14] shows experiments where a subset of 10-15 signatures from the NASA Spectral Database (400+ signatures) maintained at NASA\JSC was applied to data from United Kingdom Infrared Telescope (UKIRT). Good results were obtained when the "correct" endmember spectral signatures for the URSO where included in the library. However, if the signature of a material in the URSO is not in the library, the algorithm fits the mixed spectra using the available spectral signatures, which led to incorrect material composition determination. For instance, a solar panel spectrum was identified as an endmember in spectra collected from rocket bodies and debris pieces leading to incorrect identification and characterization in [14].

Another problem with library-based unmixing is high coherence (or similarity) between spectral signatures, which may lead to incorrect endmember identification or numerical ill-conditioning. Furthermore, the environmental conditions during collection by the sensor are quite different from those in a laboratory setting. Therefore, library spectra may differ significantly from data-based spectra even though they may represent the same material.

The capacity of discovering signatures of materials not present in the library from measured spectral data is one that will significantly contribute to better characterize URSO. Furthermore, even if the library contains the spectral signature of all satellite materials, natural variability introduced by environmental factors [15] may contribute to

incorrect material identification. Therefore, the capacity to find endmembers present in an object but not in the library and to account for material spectral variability or changes are important features for accurate URSO composition determination.

3. SIMULATION RESULTS

3.1 Simple Simulation Model

A challenge in our work has been the lack of access to hyperspectral data for algorithm testing and validation. A simple simulation model was proposed by [17] that captures some of the features being explored in this work about the use of spectro-temporal signatures for hyperspectral unmixing for determining composition that could be applicable to material composition determination for URSO. The simple simulation consist of a sphere whose surface is made of patches of different materials rotating over a background. As the ball rotates, different faces of the sphere appear in the field of view of the sensor. A temporal video trace of the ball rotating is generated. Each frame of the video is used to compute one mixed signature. The mixed signature for one frame is computed using the LMM in (1) where the endmembers correspond to selected signatures from the USGS spectral library and the corresponding abundance is equal to the fraction of pixels occupied by that material in the video frame. As the ball rotates the number of pixels corresponding to different materials change simulating the temporal mixed spectral trace that is generated by an URSO as it rotates and/or tumbles along its trajectory. This is illustrated in Fig. 1 for 12 frames. Each color in the ball is associated with a spectral signature of a material. This simple model does not consider illumination conditions and bidirectional reflectance, which are relevant and important in this problem.

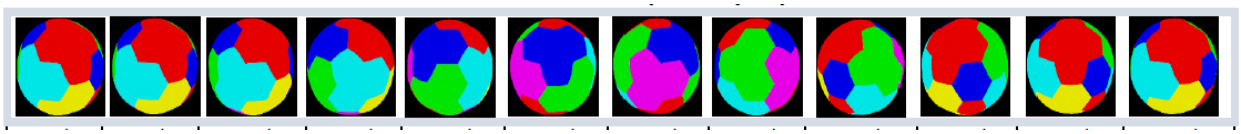

Fig. 1: Simple simulation model of a rotating ball over a background: each color in the ball is associated with a spectral signature.

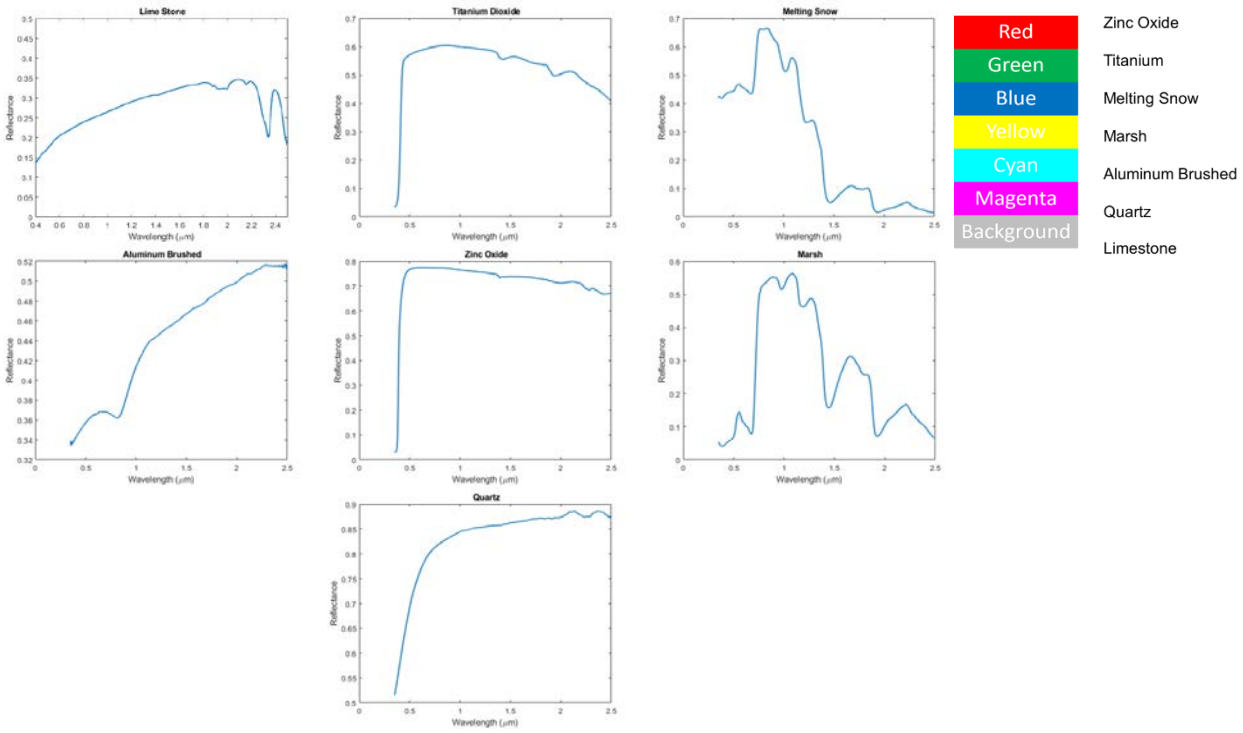

Fig. 2: Endmember spectral signatures used in the simulation, from [18].

Seven materials (one background (black) and six colors (red, green, blue, cyan, yellow, magenta) were used in the simulations presented here. Each color in the simulation is associated with the spectral signature of a material: limestone (black-background), melting snow (Blue), titanium dioxide (green), zinc oxide (red), aluminum brushed (cyan), marsh (yellow), and quartz (magenta). The spectral signatures are shown in Fig. 2 and were downloaded from USGS library [18]. These are the endmembers that we would like to extract using unmixing approaches. The computed abundances for each color are summarized in Table 1 for each frame.

Table 1: Abundance for each material at the individual video frames.

Color in the Ball	Frame Number											
	1	2	3	4	5	6	7	8	9	10	11	12
Red	0.3035	0.2942	0.2518	0.1688	0.0834	0.0671	0.0694	0.0760	0.2016	0.3258	0.3421	0.3164
Green	0.0130	0.0148	0.0369	0.1113	0.2232	0.2038	0.1726	0.3170	0.2711	0.1144	0.0341	0.0129
Blue	0.0774	0.0750	0.0735	0.1202	0.2334	0.2915	0.1857	0.0723	0.1094	0.1278	0.1008	0.0817
Cyan	0.2240	0.2379	0.2815	0.2919	0.1744	0.0254	0.0109	0.0957	0.1170	0.0893	0.1362	0.2011
Yellow	0.1214	0.1176	0.0933	0.0391	0.0048	0.0012	0.0022	0.0024	0.0155	0.0825	0.1238	0.1258
Magenta	0.0014	0.0018	0.0042	0.0073	0.0223	0.1494	0.2985	0.1780	0.0238	0.0014	0.0014	0.0012
Background	0.2592	0.2588	0.2588	0.2614	0.2586	0.2615	0.2608	0.2587	0.2615	0.2588	0.2617	0.2610

3.2 Endmember Extraction results

We applied two endmember extraction algorithms used for terrestrial applications to the simulated temporal trace of 12 mixed signatures. The first endmember extraction algorithm was SVDSS described in [19]. This algorithms assumes that the endmember signatures are contained in the data or the pure pixel assumption (which is incorrect as none of the frames contain a single material). The second algorithm in the constrained Nonnegative Matrix Factorization (cNMF) of [20], which does not assume the endmember are contained in the data and extracts virtual endmembers [21].

The spectral signatures of the extracted endmembers using SVDSS are shown in Fig. 5(a). Note that the algorithm chose a subset of seven signatures from the mixed signature set. The virtual endmembers extracted with cNMF initialized with the SVDSS endmembers are shown in Fig. 5(b). To compare the extracted and true endmembers, a 3D scatter plot of the first 3 principal components is shown in Fig. 6. In this plot the mixed signatures are points marked with x-blue, true endmembers correspond to the points marked with *-black, the virtual endmembers correspond to the points marked with *-red, and those signatures selected by SVDSS from the mixed signatures are marked with magenta circles around their blue crosses.

Clearly the extracted endmember with SVDSS or cNMF do not match the true ones. The ones from cNMF do not match the measured signatures as SVDSS and give the impression of generating a simplex with higher volume do but are still quite different from the true ones. In a way this result is not surprising, as geometric-based endmember algorithms (both SVDSS and cNMF belong to this class) search for the corners of the simplex containing the data. The extracted endmembers try to do that in a way. There are trying to find a simplex that encloses the measured data of minimum volume. The volume of the simplex containing the mixed data is much smaller than the volume spanned by the real endmember. In a way, the mixed data is not informative enough to allow us to find the real endmembers. The extracted virtual signatures result in endmembers that are not close to the true ones but enclose the actual data.

This point out to the challenge that the solution extracted by the algorithms are modulated by the assumptions and the quality of the data. The simulated data is not "rich" enough to provide information about the true endmembers. In terrestrial applications, the data cloud contains significantly more points and it is usually richer in information that allows these purely machine driven approaches to work better.

Our next step, in this work is to study how additional knowledge like partial information about the actual endmembers allow us to add additional constraints to the problem that can help data driven approaches to obtain virtual endmembers closer to the true ones.

Fig. 3: Computed mixed signatures for each video frame.

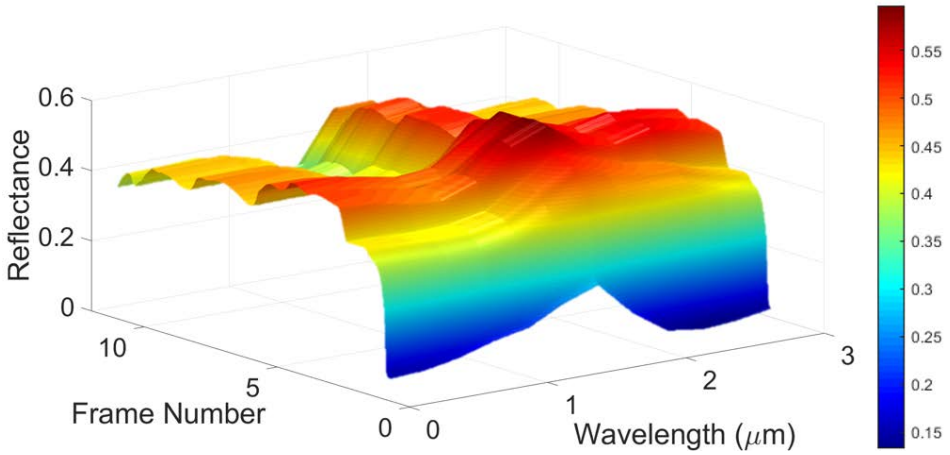

Fig. 4: Spectro-temporal signature of the rotating multi-material sphere.

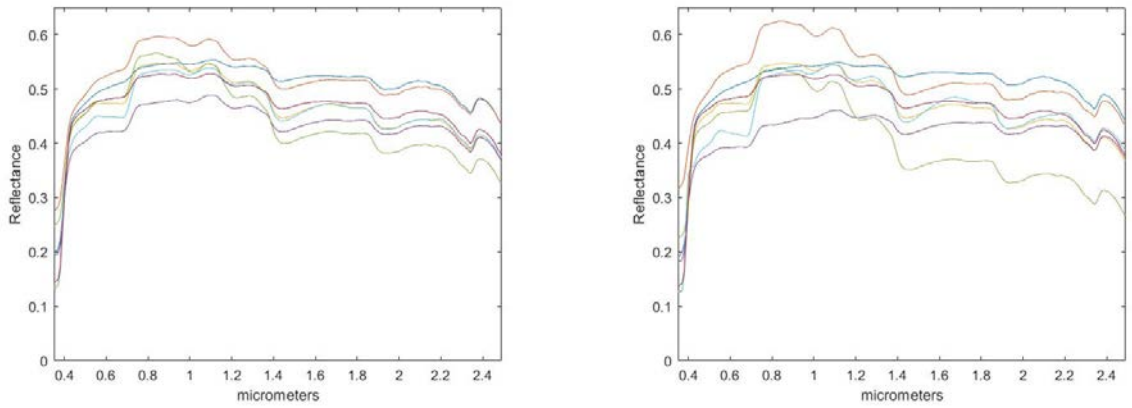

(a) (b)

Fig. 5: Retrieved endmembers using data driven approaches: (a) SVDSS, (b) cNMF.

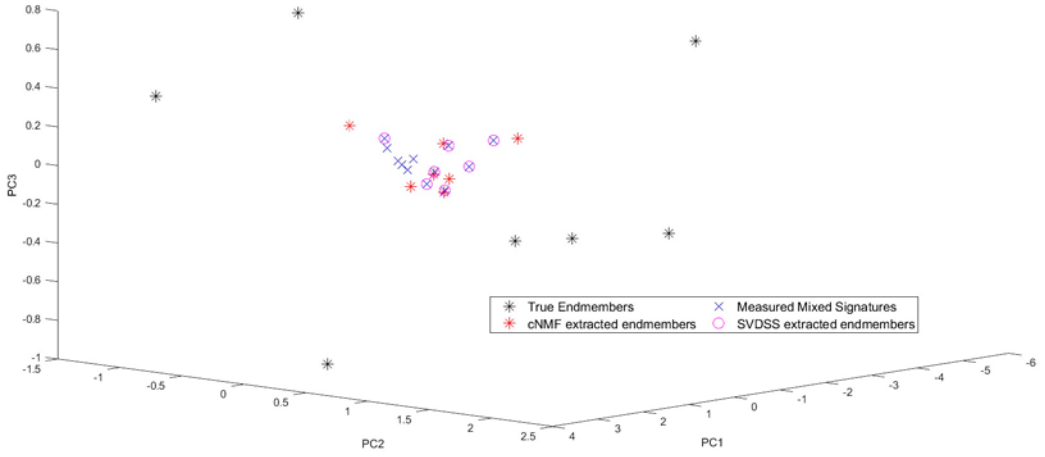

Fig. 6: 3D scatterplot in principal component coordinates for the measured mixed signatures.

4. DISCUSSION

Endmember extraction algorithms were applied to data generated by a simple simulation model that aims at providing data with some of the features in spectro-temporal traces of URSO measured by hyperspectral sensors. We can see that data-driven endmember extraction algorithms that work well with terrestrial applications may not be able to produce satisfactory results with spectro-temporal signatures of URSO. The spectro-temporal data may not be rich enough to provide enough information about the actual endmembers. In the simulation example, we can see that from the 3D scatterplot in Fig. 6 where the volume of the mixed pixels data cloud is much smaller than the volume of the simplex generated by the true endmembers. Both data driven endmember extraction approaches studied here, try to find the minimum volume simplex that encloses all the data cloud. Extracted endmembers follow that assumption but are not close to the true ones.

In the future, we will explore how partial endmember information such as that provided by spectral libraries may be used to constrain the endmember extraction program to generate more meaningful endmembers.

5. ACKNOWLEDGEMENTS

This work was supported by the Office of the US Assistant Secretary of Defense for Research and Engineering through the Research and Education Program for Historically Black Colleges and Universities and Minority-Serving

Institutions (HBCU/MI) under Award No. W911NF-19-1-0011. Opinions, interpretations, conclusions, and recommendations are those of the author and are not necessarily endorsed by the Department of Defense.

REFERENCES

[1] M,A. Baird, "Maintaining Space Situational Awareness and Taking It to the Next Level." *Air & Space Power Journal*, 50-73, 2013.

[2] D.L. Oltrogge, S. Alfano, C. Law, A. Cacioni, and T.S. Kelso, , "A Comprehensive Assessment of Collision Likelihood in Geosynchronous Earth Orbit", *Acta Astronautica*, 147:316-345, 2018.

[3] J. P. Kerekes, "Exploring Limits in Hyperspectral Unresolved Object Detection." *Proceedings of the 2011 IEEE International Geoscience and Remote Sensing Symposium*, 4415-4418, 2011.

[4] J. M. Bioucas-Dias, A. Plaza, N. Dobigeon, M. Parente, Q. Du, P. Gader, J. Chanussot, "Hyperspectral Unmixing Overview: Geometrical, Statistical, and Sparse Regression-Based Approaches," *Journal on Selected Topics in Applied Earth Observations and Remote Sensing*, 5(2): 354-379, 2012.

[5] D. L. Nishimoto, J.L. Africano, P.F. Sydney, K.M. Hamada, V.S. Hoo, P.W. Kervin, and E.G. Stansbery, "Spectroscopic observations of space objects and phenomena using Spica and Kala at AMOS" *Multifrequency Electronic/Photonic Devices and Systems for Dual-Use Applications*, 4490:212-220, 2001.

[6] J.T. Rayner, D.W. Toomey, P.M. Onaka, A.J. Denault, W.E. Stahlberger, W.D. Vacca, M.C. Cushing, and S. Wang, "SpeX: a medium-resolution 0.8-5.5 micron spectrograph and imager for the NASA infrared telescope facility", *Publications of the Astronomical Society of the Pacific*, 115(805): 362, 2003.

[7] C.L. Lawson, and R.J. Hanson, *Solving Least Squares Problems*. Society for Industrial and Applied Mathematics, 1995.

[8] S. Rosario-Torres and M. Velez-Reyes, "An algorithm for fully constrained abundance estimation in hyperspectral unmixing." *Proceedings of SPIE*, 5806:711-719, 2005.

[9] R.N. Clark, G.A. Swayze, R.Wise, K.E. Livo, T. Hoefen, R.F. Kokaly, and S.J. Sutley, *USGS Digital Spectral Library splib06a*, US Geological Survey, 2007.

[10] A.M. Baldridge, S.J. Hook, C.I. Grove, and G. Rivera, "The ASTER spectral library version 2.0." *Remote Sensing of Environment*, 113(4):711-715, 2009.

[11] H. Cowardin, S.M. Lederer, G. Stansbery, P. Seitzer, B. Buckalew, K. Abercromby, and E. Barker, "NASA's Optical Measurement Program." *Proceedings of AMOS Technical Conference*, 2004.

[12] D. Roberts, M. Gardner, R. Church, S. Ustin, G. Scheer, and R. Green, "Mapping Chaparral in the Santa Monica Mountains Using Multiple Endmember Spectral Mixture Models," *Remote Sensing of Environment*, 65:267–279, 1998.

[13] M.D. Iordache, J.M. Bioucas-Dias, and A. Plaza, "Sparse unmixing of hyperspectral data." *IEEE Transactions on Geoscience and Remote Sensing*, 49(6):2014-2039, 2011.

[14] B. Buckalew, K. Abercromby, S. Lederer, J. Frith, and H. Cowardin, "United Kingdom Infrared Telescope's Spectrograph Observations of Human-Made Space Objects," 2017. Available from: https://ntrs.nasa.gov/archive/nasa/casi.ntrs.nasa.gov/20170003832.pdf

[15] K. Abercromby, M. Guyote, J. Okada, and E. Barker, "Applying space weathering models to common spacecraft materials to predict spectral signatures." *Advanced Maui Optical and Space Surveillance Technologies Conference*, 2005.

[16] K. Abercromby, K. Hamada, M. Guyote, J. Okada, and E. Barker, "Remote and Ground Truth Spectral Measurement Comparisons." *Advanced Maui Optical and Space Surveillance Technologies Conference*, 2007.

[17] J. Yi and M. Velez-Reyes "Simplified simulation of unresolved objects in hyperspectral remote sensing for space situational awareness," *Proceedings of SPIE*, 11392, 2020.

[18] USGS, "Spectroscopy Lab", https://www.usgs.gov/labs/spec-lab (Accessed 8 December 2019)

[19] M. Velez-Reyes and M. Aldeghlawi, "Using a column subset selection method for endmember extraction in hyperspectral unmixing," *Proceedings of SPIE*, 10644, 2018.

[20] Y.M. Masalmah and M. Velez-Reyes, "A full algorithm to compute the constrained positive matrix factorization and its application in unsupervised unmixing of hyperspectral imagery," *Proceedings of SPIE*, 6966, 2008.

[21] R.A. Schowengerdt, *Remote Sensing: Models and Methods for Image Processing*, Elsevier, 2006.